How to cite: *Angew. Chem. Int. Ed.* **2023**, *62*, e202312276
doi.org/10.1002/anie.202312276

Polymer Photocatalysts

Organic Polymer Dots Photocatalyze CO_2 Reduction in Aqueous Solution

*Bin Cai[+], Martin Axelsson[+], Shaoqi Zhan[+], Mariia V. Pavliuk, Sicong Wang, Jingguo Li, and Haining Tian**

Abstract: Developing low-cost and efficient photocatalysts to convert CO_2 into valuable fuels is desirable to realize a carbon-neutral society. In this work, we report that polymer dots (Pdots) of poly[(9,9′-dioctylfluorenyl-2,7-diyl)-*co*-(1,4-benzo-thiadiazole)] (PFBT), without adding any extra co-catalyst, can photocatalyze reduction of CO_2 into CO in aqueous solution, rendering a CO production rate of 57 $\mu mol\,g^{-1}\,h^{-1}$ with a detectable selectivity of up to 100 %. After 5 cycles of CO_2 repurging experiments, no distinct decline in CO amount and reaction rate was observed, indicating the promising photocatalytic stability of PFBT Pdots in the photocatalytic CO_2 reduction reaction. A mechanistic study reveals that photoexcited PFBT Pdots are reduced by sacrificial donor first, then the reduced PFBT Pdots can bind CO_2 and reduce it into CO via their intrinsic active sites. This work highlights the application of organic Pdots for CO_2 reduction in aqueous solution, which therefore provides a strategy to develop highly efficient and environmentally friendly nanoparticulate photocatalysts for CO_2 reduction.

Introduction

Converting CO_2 into value-added green fuels is considered an effective way to provide renewable fuels to human beings and realize a carbon-neutral society. Photocatalysis is one of the methods that can directly use solar energy, water, and CO_2 to generate renewable fuels. Nevertheless, the carbon-oxygen double bond in CO_2 molecules is extremely stable,[1] and can only be directly split with ultraviolet light in normal conditions. The pioneering work of Honda and co-workers paved the way for CO_2 photoreduction under visible light with TiO_2 as the photocatalyst.[2] Subsequently, many inorganic photocatalysts such as ZnO,[3] CdS,[4] ZnS,[5] GaN,[6] and CdSe,[7] et al. have been developed and showed different selectivity and activities in photocatalytic CO_2 reduction. However, the majority of inorganic photocatalysts suffer dilemmas such as inflexible band gap modification,[8] inconvenient purification,[9] toxicity if heavy metals are contained,[10] and uncontrollable trap states,[11] etc. In contrast, the photochemical properties, energy band alignment, and solubility of organic polymer catalysts can be easily tuned by changing the monomers, thereby rendering pure organic polymers promising CO_2 reduction catalysts.[12] Therefore, during recent years, many organic polymer photocatalysts have been developed and have shown good CO_2 reduction performance, such as covalent organic frameworks (COFs),[13] C_3N_4,[14] linear polymers,[15] and porous polymers.[16] Improving the charge mobility by creating a highly conjugated polymer facilitates photogenerated charge migration to the active site where the catalysis reaction happens, therefore, represents one of the most effective polymer design strategies.[17] However, higher conjugated moieties tend to aggregate because of relatively strong π–π interactions with each other in water dispersion, thus reducing the catalyst's active sites for the reduction reaction; even though increasing the polymer porosity can increase the active surface area, it requires a finely designed polymer structure. Additionally, these reported organic photocatalysts suffer from poor dispersibility in water, where the protons and electrons could be potentially provided, coupling with water oxidation reaction. Polymer dots (Pdots) represent a subgroup of polymer nanoparticles with a particle size of less than 100 nm.[18] Making organic polymers into Pdots with amphiphilic polymer as surfactant can stabilize the organic polymer in water, enlarge surface area, and concentrate charges in a particle, which are therefore beneficial for catalytic reactions in water requiring multiple charges. Pdots have displayed promising activities in photocatalytic hydrogen production and hydrogen peroxide production.[18d] To the best of our knowledge, Pdots have not been reported for photocatalytic CO_2 reduction.

In this work, we investigated the photocatalytic activity of poly[(9,9′-dioctylfluorenyl-2,7-diyl)-*co*-(1,4-benzo-thiadiazole)] (PFBT) Pdots (avg. 40 nm, see Figure 1) for CO_2 reduction in an aqueous solution and we obtained a satisfactory CO production rate of 57 $\mu mol\,h^{-1}\,g^{-1}$ with high selectivity. For comparison, PFBT nanoparticles without

[*] Dr. B. Cai,[+] M. Axelsson,[+] Dr. M. V. Pavliuk, S. Wang, J. Li, Prof. Dr. H. Tian
Department of Chemistry-Ångström Laboratory, Uppsala University
Box 523, SE 751 20, Uppsala (Sweden)
E-mail: haining.tian@kemi.uu.se
Dr. S. Zhan[+]
Department of Chemistry-BMC, Uppsala University
BMC Box 576, S-751 23 Uppsala (Sweden)
[+] These authors contributed equally to this work.

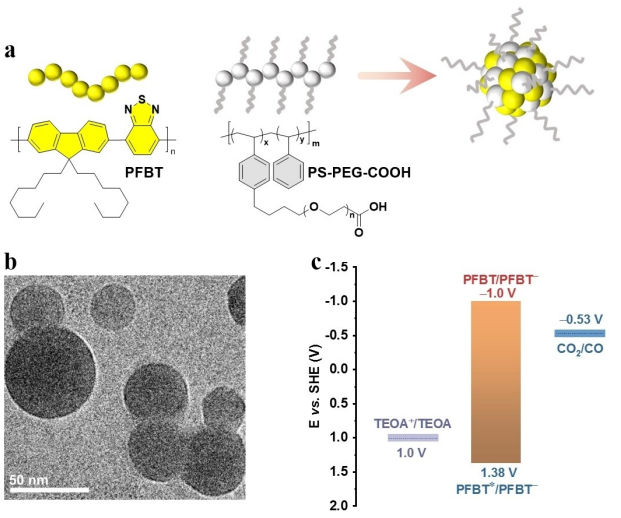

Figure 1. (a) Illustration of the structures of PFBT, PS-PEG-COOH, and the corresponding Pdots. (b) Cryo-EM micrograph of the PFBT Pdots. (c) Energy level alignment of PFBT and TEOA oxidation potential as well as CO_2 reduction potential.

surfactant (noted as "PFBT NPs", avg. 200 nm, see Figure S1) and pristine PFBT polymer (bulk material) were also tested under the same conditions. The results demonstrated the superior advantage of fabricating Pdots as the photocatalyst for CO_2 reduction. Electrochemical experiments suggest that CO_2 can bind with the reduced PFBT polymer, which then could result in an efficient photocatalytic reaction in Pdots.

Results and Discussion

The chemical structures of PFBT and amphiphilic copolymer polystyrene grafted with ethylene oxide and carboxyl groups (PS-PEG-COOH) are shown in Figure 1a. PFBT Pdots are prepared based on the reported method with a little modification,[19] and detailed procedures were illustrated in Scheme S1. Briefly, PFBT and an amphiphilic copolymer, PS-PEG-COOH were dissolved in THF and then poured into water. After slowly evaporating THF, the PFBT polymers were stabilized by PS-PEG-COOH to finally form Pdots. Determined through the UV/Vis absorption calibration curve, the PFBT content in PFBT Pdots and PFBT NPs are 41 $\mu g\,mL^{-1}$ and 51 $\mu g\,mL^{-1}$, respectively (see Figure S2). To measure the particle size and morphology of PFBT Pdots, dynamic light scattering (DLS) (Figure S3) and cryo-transmission electron microscopy (Cryo-EM) (Figure 1b and Figure S4) were performed. The Cryo-EM test reveals that PFBT Pdots possess an amorphous spherical morphology with a particle size average of 40 nm. PFBT NPs have also been prepared as a control experiment, and they have a particle size of an average of 200 nm with an ellipsoid shape determined by Scanning electron microscopy (SEM).

The UV/Vis absorption and photoluminescence (PL) emission spectra of PFBT Pdots and PFBT NPs are shown in Figure 2. For comparison, PFBT dissolved in THF as the solution and PFBT film deposited on the glass as the solid-state were also measured. It was found that the absorption of both onsets of the PFBT Pdots and PFBT NPs red-shifted compared with PFBT/THF solution, but shifted by a lesser extent compared with PFBT solid-state film. This shift is attributed to aggregation between PFBT polymers in the particles, which therefore extends the light absorption edge to 550 nm.[20] Though PFBT Pdots and PFBT NPs exhibited almost the same absorption profile, the PL spectrum of PFBT NPs red-shifted by a slightly larger degree, which could be due to the influence of their different surface chemistry environments on the PL radiative recombination processes.[21]

The prepared PFBT Pdots, PFBT NPs, and pristine PFBT bulk powder were then evaluated as the photocatalysts for CO_2 photoreduction. Typically, 0.2 M triethanolamine (TEOA) was added as the electron donor, then the sealed vial was purged with pure CO_2 for 30 minutes to reach saturation, and illuminated with an LED light (420–750 nm, 50 $mW\,cm^{-2}$). The headspace products were detected with gas chromatography (GC). As shown in Figure 3a and Figure S6, PFBT Pdots exhibited a CO production rate of 57 $\mu mol\,g^{-1}\,h^{-1}$ with a turnover number of 58 by one PFBT polymer over 5 hours calculated with a CO calibration curve (Figure S5), given that one PFBT polymer can only be single-electron reduced during the photocatalysis and assuming that all polymers in Pdots are active for catalysis. No obvious CO product was detected if one of the key components, CO_2, light, TEOA, and PFBT Pdots, was absent in the reaction, conclusively attributing the reaction to a light-driven photocatalytic process (Figures S7 and S8). PFBT NPs and pristine PFBT bulk powder (50 $\mu g\,mL^{-1}$) were tested under the same conditions, which only presented a CO production rate of 16 $\mu mol\,g^{-1}\,h^{-1}$ and 1 $\mu mol\,g^{-1}\,h^{-1}$, respectively (Figure 3a). The relatively superior catalytic performances of PFBT Pdots might be explained by a shorter exciton diffusion distance inside Pdots to the interface between Pdots and reactants, as well as a larger surface

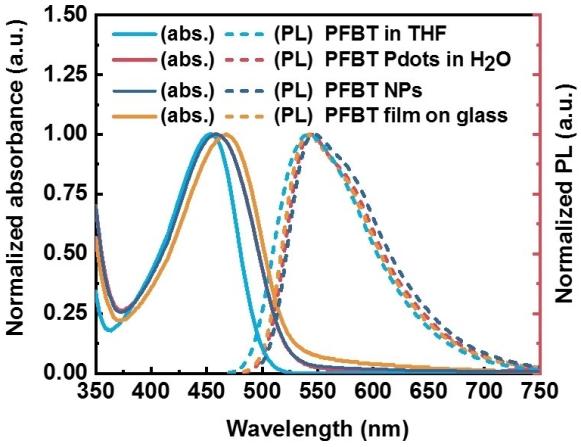

Figure 2. Normalized UV/Vis absorption and PL emission spectra of the PFBT Pdots and PFBT NPs dispersed in water, PFBT polymer dissolved in THF, and PFBT thin film deposited on glass.

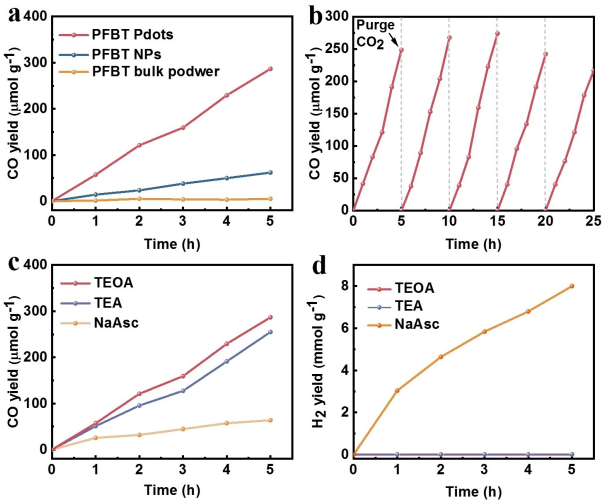

Figure 3. (a) CO production curves with different photoreduction catalysts, the red line represents adding PFBT Pdots, the blue line represents adding PFBT NPs, and the yellow line represents pristine PFBT bulk power. (b) 5 cycles of PFBT Pdots stability test by purging CO_2 every 5 hours. (c) CO production curves with different sacrificial electron donors. (d) H_2 production curves with different sacrificial electron donors, TEOA, TEA and NaAsc; all experiments were conducted with 0.2 M TEOA in the presence of CO_2 under 50 mW cm^{-2} LED white light (420–750 nm).

area due to their relatively small particle sizes. Additionally, Pdots are reported to be rich in hydrophilic channels, enabling efficient proton diffusion and benefiting CO_2 reduction.[22] When introducing aqueous solutions of PFBT Pdots and PFBT NPs at a concentration of 50 μg mL^{-1} with a certain amount of CO_2 in the headspace, the observed increases in CO_2 solubility, as compared to pure water, are 37 % and 4 %, respectively (Figure S9).[7b] Furthermore, varying quantities of PFBT Pdots were employed in CO_2 photoreduction experiments to assess the impact of concentration. It revealed that the amount of CO production exhibited a rapid escalation from 12.5 μg mL^{-1} to 50 μg mL^{-1}, ultimately reaching a plateau upon reaching a concentration of 80 μg mL^{-1}. Further increasing the concentration does not significantly improve harvesting efficiency anymore, as illustrated in Figure S10, therefore limiting further increase of CO production.

Noticeably, PFBT NPs became more blurred after CO_2 purging, which was caused by light scattering due to the relatively larger aggregate size (Figures S11 and S12). The reason is that PFBT polymer is highly hydrophobic and tends to aggregate when dispersed in water without stabilization from the surfactant. However, PFBT Pdots dispersion was kept clear and transparent, indicating their smaller and more stable particles. Zeta potential of the prepared PFBT Pdots was determined to be −12.2 mV, which makes them stable in aqueous solution for a long time (Figure S13). Further, the PFBT Pdots were purged with CO_2 after running for 5 h to reinitiate the photocatalytic reaction and were found to be still stable after 5 cycles of CO_2 re-purging experiments (Figure 3b). A small decrease in performance could be attributed to a small fraction of PFBT precipitate, stemming from the aggregation of polymers.[19] This decline should not be a result of polymer degradation, as evidenced by the absence of discernible changes in the Fourier-transform infrared spectroscopy (FT-IR), UV/Vis absorption, X-ray photoelectron spectroscopy (XPS), and PL emission spectra of PFBT before and after 20 hours reaction (Figures S14 and S15).

As PFBT Pdots have been reported to produce hydrogen in the presence of ascorbic acid in acidic conditions (pH 4),[19,23] proton reduction could be a competing reaction to CO_2 reduction. From GC detection, no obvious H_2 peak was observed after 5 hours of illumination, probably because of the basic condition used for the CO_2 reduction (Figure S16). Thus, the selectivity of CO production in gaseous products is 100 % out of CO + H_2 under this condition. Subsequently, we investigated CO_2 photoreduction with three different sacrificial electron donors: TEOA, triethylamine (TEA), and sodium ascorbate (NaAsc). As shown in Figure 3c, CO production based on TEOA exhibited a slight advantage over TEA, and a significantly superior performance compared to NaAsc. This intriguing variation could potentially be attributed to differences in pH, where the TEOA system displayed a pH of 8, the TEA system a pH of 9, and the NaAsc system a pH of 6 (Figure S17) in the presence of saturated CO_2. According to our findings, the hydrogen production from PFBT Pdots can be significantly suppressed when the photocatalytic condition goes to basic (pH 8) because the protonation of benzothiadiazole is an important step for proton reduction.[24] In the TEOA and TEA systems, H_2 production remains negligible due to the elevated pH levels, rendering the benzothiadiazole unit less effective to be protonated. However, in the NaAsc system, the competitive reaction of H_2 production emerges, driven by the favorable pH of 6 (Figure 3d). Additionally, the relatively higher pH level in the TEA system might result in a scarcity of protons, potentially contributing to a less effective CO_2 reduction process where proton participation is essential. Moreover, the liquid phase of the PFBT Pdots solution was filtered after photocatalysis and used to measure ^{1}H NMR spectroscopy in D_2O to detect liquid and highly water-soluble product such as formic acid, which is reported to be produced by organic polymer catalyst.[25] However, no formate and other products were observed (Figure S18), indicating the high selectivity of CO production with the PFBT Pdots as the CO_2 photoreduction catalyst.

To confirm that the CO was produced from CO_2 reduction rather than from polymer degradation, ^{13}C isotope labelling experiments were therefore conducted by using $^{13}CO_2$ instead of $^{12}CO_2$ for photocatalytic reaction. The products were qualitatively measured by gas chromatography-mass spectrometry (GC-MS). Only a ^{13}CO mass species (m/z = 29) was found when $^{13}CO_2$ was used to conduct CO_2 photoreduction. The absence of m/z = 28 species indicated that the produced CO indeed came from CO_2 reduction since the CO peak was detected even using $^{13}CO_2$ to conduct CO_2 photoreduction (Figure 4a,b, and Figure S19).

The residual Pd has been suggested to be an active site for proton reduction in organic polymers synthesized from

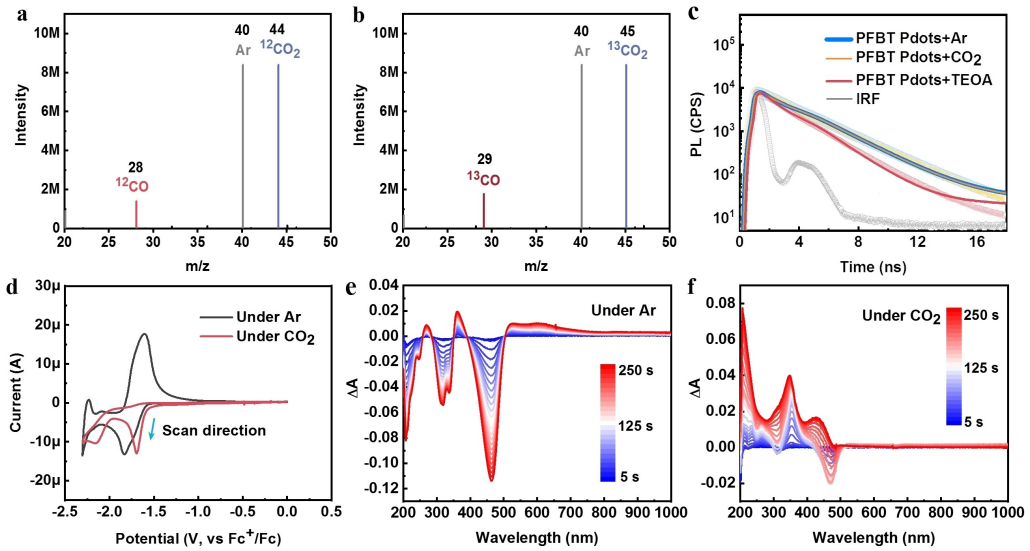

Figure 4. GC-MS measurements of the headspace for PFBT Pdots CO_2 photoreduction under (a) purging with $^{12}CO_2$, (b) purging with $^{13}CO_2$. (c) Time-related PL decay of the PFBT Pdots in water when purging with Ar (green circle, noted as "PFBT + Ar"), CO_2 (yellow circle, noted as "PFBT + CO_2"), and adding TEOA under Ar (purple circle, noted as "PFBT + TEOA"). (d) CV curves of the PFBT in THF when purging with Ar or CO_2, 0.1 M TBAF as the supporting electrolyte, glassy carbon as the working electrode, Pt wire as the counter electrode, $Ag/AgNO_3$ as the reference electrode, under a scan speed of 50 mV s^{-1}; Spectroelectrochemistry of the PFBT measured in THF, with a bias of −2.0 V vs. Fc^+/Fc, with Pt mesh as the working electrode, Pt wire as the counter electrode, $Ag/AgNO_3$ as the reference electrode, 0.1 M TBAF as the supporting electrolyte under (e) Ar, (f) CO_2 atmosphere.

the Suzuki coupling reaction.[26] To investigate the influence of Pd in PFBT Pdots for CO_2 reduction, we conducted CO_2 photocatalytic reduction experiments using PFBT Pdots with varying Pd content. These content variations included pristine PFBT containing 24 ppm Pd, the washed PFBT with Pd content below the detection limit (< 1 ppm) of inductively coupled plasma-optical emission spectroscopy (ICP), and PFBT enriched with an additional 9 wt% Pd. As depicted in Figure S20, no substantial distinctions were evident among the different groups. The results suggest that if Pd is indeed a catalytic site in PFBT Pdots photocatalysts for CO_2 reduction, then only "negligible" chemically bound Pd (< 1ppm) is needed for this reaction.[27]

Upon excitation, PFBT* could transport the hole to TEOA by reduction quenching, or transport electrons to CO_2 by oxidation quenching in the first step, judging from their energy band alignments in Figure 1c (calculation details are provided in Figure S21). Time-correlated single photon counting (TCSPC) measurements of the PFBT Pdots measured in water by purging Ar or CO_2, as well as adding TEOA under Ar, were then compared (Figure 4c). No obvious change in the PL lifetime was observed when purging CO_2 compared with purging Ar (inert condition). However, the PL lifetime of PFBT decreased from 2.42 ns to 1.79 ns when TEOA was introduced under the Ar conditions, which indicates that excited PFBT goes to the reductive quenching by TEOA initially.

To further investigate the interaction between reduced-state PFBT and CO_2, cyclic voltammetry (CV) measurements of the PFBT in THF were conducted under Ar and CO_2 atmospheres, respectively (Figure 4d). Compared with CV measured in the Ar atmosphere, PFBT reduction peaks positively shifted after purging CO_2 and became irreversible. Moreover, obvious differences in spectroelectrochemistry (SEC) of PFBT measured in THF under Ar and CO_2 conditions were also observed (at a bias of −2.0 V vs Fc^+/Fc, Figure 4e,f). When in Ar conditions, the absorption decrease minimum is observed at around 200 nm, 320 nm, and 450 nm (ascribed to the PFBT ground state bleach) and the absorption increase maximum at around 270 nm, 360 nm, and 600 nm (attributed to the PFBT reduced state). Additionally, the SEC profile measured under the CO_2 conditions before 25 s closely resembles that obtained in the Ar conditions, which indicates the generation of a PFBT reduced state (Figure 4f and Figure S22). However, new absorption peaks increase maximum (observed at around 200 nm, 350 nm, and 430 nm) emerged as time evolved, and the SEC profile exhibited an enormous difference to that obtained under the Ar conditions with the disappearance of reduced-state PFBT characteristics, which suggests the interaction between the reduced-state PFBT with CO_2.

However, no CO was detected from bulk electrolysis at a potential of −2.0 V (vs Fc^+/Fc) under a CO_2 atmosphere for 1 hour. This phenomenon could potentially arise from the distinct chemical environment inherent to Pdots, as compared to individual polymer in THF. To illustrate this chemical environment impact, we calculated the reaction energy of CO_2 reduction based on PFBT Pdots and PFBT polymer. As one PFBT can only be single-electron reduced during photocatalysis, we simplified our analysis by representing one PFBT polymer using a repeating block unit. Moreover, guided by reports that reduced benzothiadiazole exhibits interaction with CO_2 as evident from IR spectra,[28] we adopted the perspective that benzothiadiazole could

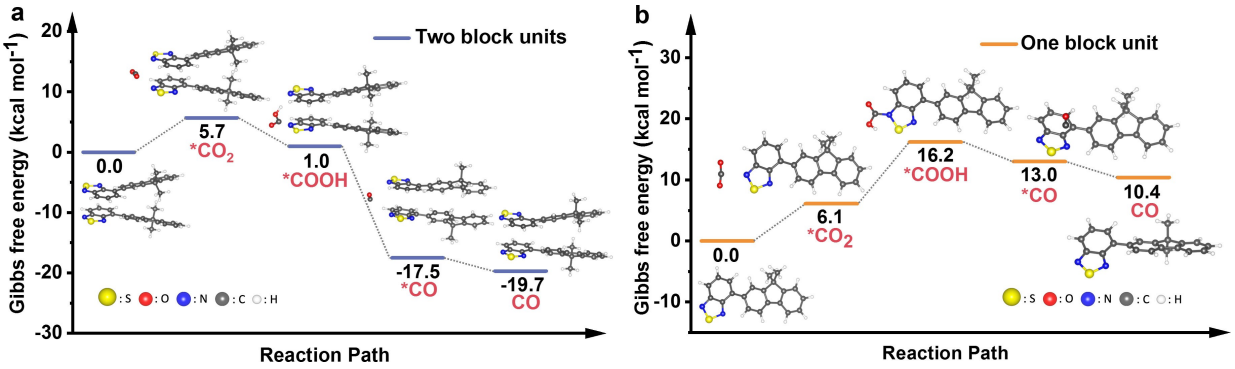

Figure 5. The energy panel of the reaction pathway on (a) the two adjacent reduced block units; (b) the one block unit.

serve as the active site in Pdots, particularly because several recently reported heteroatomic organic molecules have shown electrocatalytic CO_2 reduction.[29]

Considering that the excited PFBT undergoes reductive quenching first, our DFT calculations were strategically initiated from the standpoint of the reduced polymer, exemplified by the reduced repeating block unit. To simulate the confined micro-environment in Pdots, where numerous PFBT polymer molecules are compacted within a small sphere, we examined the reaction energy under two different scenarios: 1) where one block unit is represented as a PFBT polymer, and 2) where two adjacent block units are represented as PFBT Pdots (Figure S23). The CO_2 reduction reaction catalyzed by two adjacent reduced block units showed the highest uphill free energy of 5.7 kcal mol^{-1} at the CO_2 adsorption and an overall reaction free energy of -19.7 mol^{-1} (Figure 5a). Conversely, the reaction catalyzed by only one reduced block unit exhibited the highest uphill free energy of up to 10.1 kcal mol^{-1} at the 1st hydrogenation step, and an overall reaction free energy of 10.4 kcal mol^{-1} (Figure 5b). The large difference in free energy between the two reaction profiles is observed in the 1st and 2nd hydrogenation steps. Specifically, within the two adjacent reduced block units, the 1st and 2nd hydrogenation steps had a free energy decrease of -4.7 kcal mol^{-1} and -18.5 kcal mol^{-1}, respectively. While in the one block unit, the corresponding steps showed an energy change of 10.1 kcal mol^{-1} and -3.2 kcal mol^{-1}, respectively. Thus, the two adjacent reduced block units containing two electrons would favor the hydrogenation steps, thereby lowering its reaction free energy, compared to the scenario of the one block unit. Based on these results, we propose that the micro-environment in Pdots facilitates CO_2 reduction, enabling the potential provision of multiple electrons for the process.

Conclusion

In summary, organic PFBT polymer dots (Pdots) were investigated for photocatalytic CO_2 reduction for the first time. Without additional co-catalyst, PFBT Pdots exhibited a high selectivity of CO production up to 100 % and a production rate of 57 μmol g^{-1}h^{-1} with TEOA as the electron donor in water, which is ca. 2 orders of magnitude higher than that produced from pristine PFBT polymers. Moreover, the prepared Pdots photocatalyst was relatively stable after 5 cycles of CO_2 re-purging experiments. The electrochemical experiment suggests that CO_2 can interact well with PFBT polymer once the PFBT polymer is reduced. And isotopic labeling experiments proved that CO was produced from CO_2 reduction rather than from polymer degradation. Although the involvement of residual Pd in the photocatalytic process cannot be completely ruled out due to the detection limit (<1ppm) of the ICP experiment, DFT calculations suggested that the micro-environment in Pdots indeed facilitates the CO_2 reduction reaction, enabling the provision of multiple electrons for photocatalytic reduction through benzothiadiazole units. This study demonstrates that Pdots can be a type of photocatalyst that can render highly efficient and selective CO_2 photoreduction in aqueous conditions, which paves the road to developing new organic polymeric photocatalysts for CO_2 reduction and studying the effect of polymer structures in Pdots on photocatalytic performance and selectivity of CO_2 reduction.

Acknowledgements

We thank the K&A Wallenberg Foundation (Wallenberg Academy Fellow program grant 2019.0156 for financial support. We would like to thank Dr. Leandro Cid Gomes for his help with GC-MS and Dr. Haoliang Cheng for the discussion. Also, we would like to acknowledge the use of the Cryo-EM Uppsala facility for cryogenic electron microscopy measurement. All DFT calculations were performed on resources provided by the Swedish National Infrastructure for Computing (SNIC) (allocations SNIC 2022-5-650) at the National Supercomputing Center in Linköping, Sweden.

Conflict of Interest

The authors declare no conflict of interest.

Data Availability Statement

The data that support the findings of this study are available from the corresponding author upon reasonable request.

Keywords: CO Production · CO_2 Photoreduction · Photocatalyst · Photochemistry · Polymer Dots

[1] G. Glockler, *J. Phys. Chem.* **1958**, *62*, 1049–1054.
[2] T. Inoue, A. Fujishima, S. Konishi, K. Honda, *Nature* **1979**, *277*, 637–638.
[3] a) M. Sayed, F. Xu, P. Kuang, J. Low, S. Wang, L. Zhang, J. Yu, *Nat. Commun.* **2021**, *12*, 4936; b) X. Liu, L. Ye, S. Liu, Y. Li, X. Ji, *Sci. Rep.* **2016**, *6*, 38474.
[4] a) H. Inoue, R. Nakamura, H. Yoneyama, *Chem. Lett.* **1994**, *23*, 1227–1230; b) N. Wang, S. Cheong, D. Yoon, P. Lu, H. Lee, Y. K. Lee, Y. S. Park, D. C. Lee, *J. Am. Chem. Soc.* **2022**, *144*, 16974–16983.
[5] a) M. Kanemoto, T. Shiragami, C. J. Pac, S. Yanagida, *J. Phys. Chem.* **1992**, *96*, 3521–3526; b) Y. X. Meng, G. P. Liu, G. F. Zuo, X. G. Meng, T. Wang, J. H. Ye, *Nanoscale* **2022**, *14*, 14455–14465.
[6] B. AlOtaibi, S. Z. Fan, D. F. Wang, J. H. Ye, Z. T. Mi, *ACS Catal.* **2015**, *5*, 5342–5348.
[7] a) C. D. Sahm, E. Mates-Torres, N. Eliasson, K. Sokolowski, A. Wagner, K. E. Dalle, Z. Huang, O. A. Scherman, L. Hammarstrom, M. Garcia-Melchor, E. Reisner, *Chem. Sci.* **2021**, *12*, 9078–9087; b) J. Wu, B. Y. Deng, J. Liu, S. R. Yang, M. D. Li, J. Li, F. Wang, *ACS Appl. Mater. Interfaces* **2022**, *14*, 29945–29955.
[8] H. Abdullah, M. M. R. Khan, H. R. Ong, Z. Yaakob, *J. CO2 Util.* **2017**, *22*, 15–32.
[9] N. Gao, X. Fang, *Chem. Rev.* **2015**, *115*, 8294–8343.
[10] V. De Matteis, *Toxics* **2017**, *5*, 29.
[11] B. Wang, G. M. Biesold, M. Zhang, Z. Lin, *Chem. Soc. Rev.* **2021**, *50*, 6914–6949.
[12] a) S. Chatani, C. J. Kloxin, C. N. Bowman, *Polym. Chem.* **2014**, *5*, 2187–2201; b) J. W. Jung, J. W. Jo, E. H. Jung, W. H. Jo, *Org. Electron.* **2016**, *31*, 149–170; c) T. Banerjee, F. Podjaski, J. Kröger, B. P. Biswal, B. V. Lotsch, *Nat. Rev. Mater.* **2021**, *6*, 168–190; d) Y.-Z. Cheng, X. Ding, B.-H. Han, *ChemPhotoChem* **2021**, *5*, 406–417.
[13] a) K. Lei, D. Wang, L. Ye, M. Kou, Y. Deng, Z. Ma, L. Wang, Y. Kong, *ChemSusChem* **2020**, *13*, 1725–1729; b) S. Wang, X. Hai, X. Ding, S. Jin, Y. Xiang, P. Wang, B. Jiang, F. Ichihara, M. Oshikiri, X. Meng, Y. Li, W. Matsuda, J. Ma, S. Seki, X. Wang, H. Huang, Y. Wada, H. Chen, J. Ye, *Nat. Commun.* **2020**, *11*, 1149.
[14] a) J. Khan, Y. Sun, L. Han, *Small Methods* **2022**, *6*, 2201013; b) J. Mao, T. Peng, X. Zhang, K. Li, L. Ye, L. Zan, *Catal. Sci. Technol.* **2013**, *3*, 1253–1260.
[15] S. H. Wang, F. Khurshid, P. Z. Chen, Y. R. Lai, C. W. Cai, P. W. Chung, M. Hayashi, R. J. Jeng, S. P. Rwei, L. Wang, *Chem. Mater.* **2022**, *34*, 4955–4963.
[16] a) C. Dai, L. Zhong, X. Gong, L. Zeng, C. Xue, S. Li, B. Liu, *Green Chem.* **2019**, *21*, 6606–6610; b) L. Hou, G. Tang, H. Huang, S. Yin, B. Long, A. Ali, G. J. Deng, T. Song, *J. Mater. Chem. A* **2022**, *10*, 5287–5294.
[17] a) S. Fratini, M. Nikolka, A. Salleo, G. Schweicher, H. Sirringhaus, *Nat. Mater.* **2020**, *19*, 491–502; b) Y. Li, Y. Zou, *Adv. Mater.* **2008**, *20*, 2952–2958.
[18] a) C. Wu, D. T. Chiu, *Angew. Chem. Int. Ed.* **2013**, *52*, 3086–3109; b) J. Yu, Y. Rong, C. T. Kuo, X. H. Zhou, D. T. Chiu, *Anal. Chem.* **2017**, *89*, 42–56; c) L. Guo, J. Ge, P. Wang, *Photochem. Photobiol.* **2018**, *94*, 916–934; d) M. V. Pavliuk, S. Wrede, A. Liu, A. Brnovic, S. Wang, M. Axelsson, H. Tian, *Chem. Soc. Rev.* **2022**, *51*, 6909–6935.
[19] L. Wang, R. Fernández Terán, L. Zhang, D. L. A. Fernandes, L. Tian, H. Chen, H. Tian, *Angew. Chem. Int. Ed.* **2016**, *55*, 12306–12310.
[20] A. Ledesma-Juárez, M. Rodríguez, M. Güizado-Rodríguez, D. Romero-Borja, C. Garcias-Morales, J. L. Maldonado, V. Barba, *J. Mater. Sci. Mater. Electron.* **2019**, *30*, 13974–13983.
[21] F. M. Winnik, S. T. A. Regismond, *Colloids Surf. A* **1996**, *118*, 1–39.
[22] A. Liu, C. W. Tai, K. Holá, H. Tian, *J. Mater. Chem. A* **2019**, *7*, 4797–4803.
[23] P. B. Pati, G. Damas, L. Tian, D. L. A. Fernandes, L. Zhang, I. B. Pehlivan, T. Edvinsson, C. M. Araujo, H. Tian, *Energy Environ. Sci.* **2017**, *10*, 1372–1376.
[24] M. Axelsson, Z. Xia, S. Wang, M. Cheng, H. Tian, *ChemRxiv preprint* **2023**, https://doi.org/10.26434/chemrxiv-2023-z6vd7.
[25] Y. Fu, D. Sun, Y. Chen, R. Huang, Z. Ding, X. Fu, Z. Li, *Angew. Chem. Int. Ed.* **2012**, *51*, 3364–3367.
[26] M. Sachs, H. Cha, J. Kosco, C. M. Aitchison, L. Francàs, S. Corby, C. L. Chiang, A. A. Wilson, R. Godin, A. Fahey Williams, A. I. Cooper, R. S. Sprick, I. McCulloch, J. R. Durrant, *J. Am. Chem. Soc.* **2020**, *142*, 14574–14587.
[27] a) A. S. Al-Janabi, W. A. Al-Jumaili, T. S. Saeed, O. A. Abd, E. Sinn, *Mater. Today: Proc.* **2021**, *43*, 977–985; b) M. Nasrollahzadeh, M. Sajjadi, H. Ghafuri, N. S. S. Bidgoli, A. J. Pombeiro, S. Hazra, *Coord. Chem. Rev.* **2021**, *446*, 214132.
[28] G. Iijima, J. Naruse, H. Shingai, K. Usami, T. Kajino, H. Yoto, Y. Morimoto, R. Nakajima, T. Inomata, H. Masuda, *Energy Fuels* **2023**, *37*, 2164–2177.
[29] a) C. H. Lim, S. Ilic, A. Alherz, B. T. Worrell, S. S. Bacon, J. T. Hynes, K. D. Glusac, C. B. Musgrave, *J. Am. Chem. Soc.* **2019**, *141*, 272–280; b) P. Karak, S. K. Mandal, J. Choudhury, *J. Am. Chem. Soc.* **2023**, *145*, 7230–7241.

Manuscript received: August 22, 2023
Accepted manuscript online: September 20, 2023
Version of record online: October 5, 2023